Resonant Auger decay of the core-excited C*O molecule in intense x-ray laser fields

Philipp V. Demekhin,* Ying-Chih Chiang, and Lorenz S. Cederbaum
Theoretische Chemie, Physikalisch-Chemisches Institut, Universität Heidelberg, Im Neuenheimer Feld 229, D-69120 Heidelberg, Germany
(Received 11 May 2011; published 26 September 2011)

The dynamics of the resonant Auger (RA) process of the core-excited $C^*O(1s^{-1}\pi^*, v_r = 0)$ molecule in an intense x-ray laser field is studied theoretically. The theoretical approach includes the analog of the conical intersections of the complex potential energy surfaces of the ground and "dressed" resonant states due to intense x-ray pulses, taking into account the decay of the resonance and the direct photoionization of the ground state, both populating the same final ionic states coherently, as well as the direct photoionization of the resonance state itself. The light-induced nonadiabatic effect of the analog of the conical intersections of the resulting complex potential energy surfaces gives rise to strong coupling between the electronic, vibrational, and rotational degrees of freedom of the diatomic CO molecule. The interplay of the direct photoionization of the ground state and of the decay of the resonance increases dramatically with the field intensity. The coherent population of a final ionic state via both the direct photoionization and the resonant Auger decay channels induces strong interference effects with distinct patterns in the RA electron spectra. The individual impact of these physical processes on the total electron yield and on the $CO^+(A\,^2\Pi)$ electron spectrum are demonstrated.

DOI: 10.1103/PhysRevA.84.033417 PACS number(s): 33.20.Xx, 32.80.Hd, 41.60.Cr, 82.50.Kx

I. INTRODUCTION

Recently, the resonant Auger (RA) decay of atoms exposed to strong x-ray laser pulses has been studied theoretically [1–4]. It has been demonstrated that under the extreme field conditions provided by x-ray free electron lasers (XFELs) [5,6], such as unprecedented high-intensity, $\sim 10^{18}$ W/cm^2, and very short pulse durations, 10–500 fs, the stimulated emission from the resonance back to the ground state starts to compete with the Auger decay. The interplay between the resonant excitation and stimulated emission results in Rabi oscillations between the ground state and the resonance within its Auger decay lifetime and pulse duration. This leads to spectacular modifications of the RA spectra, like the appearance of multipeak structure in the electron spectra [1,2]. It has also been demonstrated [2–4] that direct photoionizations of the ground state and of the resonant state increase dramatically with the field intensity, resulting in additional leakages of the corresponding populations into all possible final ionic states. Moreover, a final ionic state is populated coherently by both the direct photoionization from the ground state and by the resonant Auger decay inducing strong interference effects with distinct patterns in the RA electron spectra of atoms [4].

What happens when a diatomic molecule is exposed to a strong laser pulse with a carrier frequency which fits to the energy difference between two electronic states? It has been demonstrated that the two resulting "dressed" electronic states exhibit a conical intersection in the space of the rotational angle and the internuclear distance [7,8]. The emergence of this light-induced conical intersection leads to substantial nonadiabatic effects and to a strong mixing of rotations and vibrations [8]. Very recently [9], the RA process in molecules in intense x-ray laser fields has been studied theoretically. Also, here it has been demonstrated that an atomiclike picture (fixed internuclear distance and molecular orientation) is inapplicable. Not only the vibrational motion plays a role in the decay as in the case of weak fields, but the rotational motion becomes very important in strong fields as well. In particular, the appearance of the analog of conical intersections of the now complex (owing to a finite lifetime of the electronic decaying state) potential energy surfaces (PESs) of the ground and "dressed" resonant states has been predicted in Ref. [9]. This phenomenon gives rise to strong nonadiabatic coupling and to strong mixing between the electronic, vibrational, and rotational degrees of freedom of diatomic molecules exposed to strong x-ray laser pulses. To demonstrate the nonadiabatic effects, the resonant ionization channel (i.e., excitation and decay of the resonance) has been explicitly included in the numerical calculations of the RA process in the HCl molecule studied in Ref. [9], whereas the leakages and interference effects mentioned above for atoms were not taken into account explicitly for transparency of presentation.

In the present work, we study how the combined action of all the aforementioned competing processes evoked by a strong field influence the multidimensional dynamics of the RA effect in diatomic molecules exposed to strong x-ray laser pulses. For this purpose, we unify the previously developed theoretical approaches for RA in atoms [4] and for molecules [9]. As demonstrated in Ref. [4], the simultaneous effect of the RA decay and of the direct ionization of the involved states results in additional modifications of the Hamiltonian governing the nuclear dynamics on the coupled dressed surfaces. One can expect that these modifications will even further enhance the nonadiabatic effects caused by the appearance of the analog of a conical intersection of the complex PESs. In our previous study [9], the case of excitation of the dissociative $HCl^*(2p^{-1}\sigma^*)$ resonant state and its subsequent RA decay into one of the dissociative final states has been investigated. There, the nuclear dynamics accompanying the RA decay result in the fragmentation of the HCl molecule, and, as a consequence, a rather simple RA spectrum appears. The RA decay of the $HCl^*(2p^{-1}\sigma^*)$ state is, however, difficult to study experimentally, owing to many overlapping intermediate and

*philipp.demekhin@pci.uni-heidelberg.de; on leave from: Rostov State Transport University, Narodnogo Opolcheniya square 2, 344038, Rostov-on-Don, Russia.

final electronic states. In the present work, we concentrate on the nuclear dynamics accompanying the RA decay of a bound resonant electronic state into a bound final ionic state of a diatomic molecule, where the corresponding vibrational structures can be resolved in the excitation and decay spectra.

The RA decay of the core-excited $C^*O(1s^{-1}\pi^*)$ molecule is a perfect candidate for our purposes. First of all, for weak fields it is one of the most thoroughly studied processes, both experimentally [10–18] and theoretically [14–21]. Therefore, all parameters for the calculations are available. Second, the weak-field excitation spectrum of the core-excited resonance consists of three well-resolved vibrational states, $v_r = 0, 1$, and 2, with excitation probabilities of about 87%, 12%, and 1%, respectively [15,18]. The energy separation of $\omega_e = 250$ meV [15] between the v_r levels of the C^*O resonance, is about three times larger than their natural lifetime width of $\Gamma_{\rm Aug} = 80$ meV [22], and thus the underlying so called lifetime vibrational interference (LVI, [23]) effects are small. The timescale of the nuclear vibrational motion, $\tau_v = 2\pi/\omega_e \approx 16.5$ fs, and that of the RA decay, $\tau_d = 1/\Gamma_{\rm Aug} \approx 8.2$ fs, are rather comparable. All of these imply that one can expect measurable fingerprints of the nuclear dynamics in the core-excited state when studying strong-field effects. Finally, the RA electron spectra corresponding to the decay of the resonance to the three lowest X, A, and B states of the CO^+ ion do not overlap (the energy separations are about 2 eV [12,17]), and can thus be studied separately. In the present work we investigate the RA decay into the $CO^+(A\,^2\Pi)$ final ionic state, which exhibits the richest vibrational structure of all the electron spectra in the weak-field case [12,17].

II. THEORY

The processes relevant to the present study are represented schematically in Fig. 1. The strong x-ray laser field with the photon energy ω around 287.4 eV couples the ground and the resonance states. As demonstrated in Ref. [9], this coupling leads to damped Rabi oscillations of the nuclear wave packets between the ground state and the resonance. The $CO^+(A\,^2\Pi)$ final ionic state can be coherently populated via the participator Auger decay of the resonance and by the direct photoionization from the ground state. The first channel is operative at those times when the wave packet is in the resonant state, and the second channel—when it is in the ground state. In addition, there are two mechanisms of losses relevant to the RA effect in strong fields. The total photoionizations of the ground state and of the resonance lead to leakages of the respective wave packets, as indicated in Fig. 1, by the vertical helix arrows from the ground state and from the resonance, respectively. These processes, except of the Auger decay itself, are operative only when the pulse is on. After the pulse expires, the final population of the ground state can be much smaller than 1. In the presence of a strong pulse, multiple ionization of a molecule takes place as well [6]. Different possibilities for that were discussed in Ref. [4]. However, multiple ionization processes, in principle, can be experimentally separated from the RA effect as soon as one measures energies of ejected electrons and does not intend to measure ions.

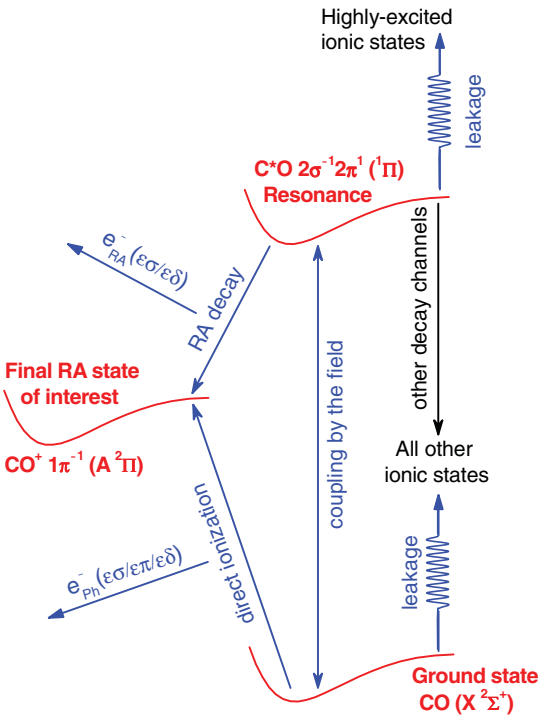

FIG. 1. (Color online) Schematic representation of RA effect of the CO molecule exposed to strong x-ray pulses (see text for details).

The currently operating XFEL, linac coherent light source (LCLS), do not produce, so far, a monochromatic radiation, and the x-ray pulses consist of many spikes with random fluctuations of the frequency, phase, and amplitude [5,6]. The impact of these problems on the RA effect of atoms has been studied in Ref. [1]. In addition, the x-ray pulse is reshaped during the propagation through a resonant medium [2,3]. In order to reveal the individual contributions of all included physical processes, we concentrate here on the physics a single molecule undergoes when exposed to a coherent and monochromatic x-ray pulse. For simplicity, we assume a Gaussian-shaped pulse of duration τ centered at t_0 [$g(t) = e^{-(t-t_0)^2/\tau^2}$] with linear polarization of the field along the z axis:

$$\mathcal{E}(t) = \mathcal{E}_0(t)\cos\omega t = \mathcal{E}_0\, g(t)\cos\omega t. \qquad (1)$$

Here, $\mathcal{E}_0$ is the peak amplitude, and the pulse-shape function $g(t)$ varies slowly on the timescale of $2\pi/\omega$. The cycle-averaged intensity of the field is given in atomic units via (1 a.u. $= 6.43641 \times 10^{15}$ W/cm^2)

$$I(t) = \frac{1}{8\pi\alpha}\{\mathcal{E}_0\, g(t)\}^2, \qquad (2)$$

where $\alpha = 1/137.036$ is the fine structure constant. For brevity of presentation, the following terminology is used throughout the manuscript. A pulse of a peak intensity well below 1 a.u. (6.43641×10^{15} W/cm^2) is referred to hereafter as a weak pulse. A weak field does not induce noticeable Rabi oscillations (leads to negligibly small stimulated emission) and can be treated perturbatively. Pulses with peak intensities comparable to or larger than 1 a.u. are referred to hereafter

as strong pulses. Strong fields govern photon absorption processes in the extremely nonlinear regime, e.g., by Rabi oscillations [1,4].

To describe the dynamics of the RA effect theoretically as a function of time, one needs to solve the time-dependent Schrödinger equation for the molecule and its interaction with the field (atomic units $e = m_e = \hbar = 1$ are used throughout)

$$i\dot{\Psi}(t) = \hat{H}(t)\Psi(t) = \left[\hat{H}_{nuc} + \hat{H}_{el} + \hat{D}\,\mathcal{E}(t)\right]\Psi(t), \quad (3)$$

where $\hat{D}$ represents the dipole transition operator. The present approach to solve Eq. (3) combines those reported in Refs. [4,9,24].

A. Nuclear dynamics Hamiltonian

We start with the randomly oriented rotating CO molecule in its ground rovibronic state $CO(X\,^1\Sigma^+, v_0 = 0, J_0 = 0)$, i.e., with an isotropic distribution over the rotational angle. We shall demonstrate below that the nonadiabatic effects of coupling the vibrational and rotational degrees of freedom of diatomic molecules induced by the laser field will change this distribution dramatically. Following Ref. [24], the total wave function of a rotating molecule as a function of time can be represented via the following ansatz, including three electronic states: the ground state and the resonance with the electronic wave functions Φ_I and Φ_R, respectively, and the final ionic state $CO^+(A\,^2\Pi)$ plus outgoing electron of energy ε with the total electronic wave function Φ_A^ε:

$$\Psi(t) = |\Psi_I(t)\rangle\Phi_I + |\widetilde{\Psi}_R(t)\rangle\Phi_R + \int |\widetilde{\Psi}_A(\varepsilon,t)\rangle\Phi_A^\varepsilon d\varepsilon. \quad (4)$$

Here, $|\Psi_I(t)\rangle$, $|\widetilde{\Psi}_R(t)\rangle$, and $|\widetilde{\Psi}_A(\varepsilon,t)\rangle$ are the time-dependent wave packets propagating on the PESs of the ground, resonant, and final ionic states, respectively. It should be remembered that these wave packets depend explicitly on the nuclear coordinates R and θ. For brevity, we will explicitly show the dependence on the nuclear coordinates only in the final Hamiltonian matrix Eq. (7) governing the nuclear dynamics.

In order to obtain the final set of equations for the propagation of the nuclear wave packets, we substitute the ansatz Eq. (4) in the time-dependent Schrödinger Eq. (3) and project the result onto each electronic state. Similarly to Refs. [4,9,24], we imply the rotating wave approximation [25], the local approximation [26,27], and redefine ("dress") the time-dependent wave packets of the resonant and final ionic states as follows:

$$|\Psi_R(t)\rangle = |\widetilde{\Psi}_R(t)\rangle\, e^{+i\omega t} \text{ and } |\Psi_A(\varepsilon,t)\rangle = |\widetilde{\Psi}_A(\varepsilon,t)\rangle\, e^{+i\omega t}. \quad (5)$$

Utilizing the rotating wave and the local approximations is well justified for high-energy resonant processes considered here [1,4]. Details of the derivation can be found in Refs. [4,9,24].

In order to derive the final Hamiltonian matrix for the nuclear dynamics accompanying the studied process, we notice that the final ionic state $CO^+(A\,^2\Pi)$ can be populated via Auger decay of the resonance by the emission of either $\varepsilon\sigma$ or $\varepsilon\delta$ RA electrons (as indicated in Fig. 1). These channels form the $^1\Pi$ symmetry of the overall final state of the ion plus RA electron, which is the symmetry of the resonant state. Contrary to that, the direct population of the $CO^+(A\,^2\Pi)$ state from the ground state may proceed via the emission of $\varepsilon\sigma$, $\varepsilon\pi$, or $\varepsilon\delta$ photoelectrons (see Fig. 1). The direct photoionization channels with $\varepsilon\sigma$ and $\varepsilon\delta$ photoelectrons contribute to the same overall final state as the resonant channels, which thus superimpose and interfere. Emission of $\varepsilon\pi$ photoelectrons, however, results in the overall final state of $^1\Sigma^+$ symmetry, which cannot be populated resonantly. Moreover, as will be shown below, these transitions are operative via different components of the dipole transition operator $\hat{D}$. That is why it is important to separate the final states explicitly in the ansatz Eq. (4) [the last integral in Eq. (4) includes both types of final states].

Let us collect the individual nuclear wave packets contributing to the total wave function Eq. (4) into a single vector

$$|\overline{\Psi}(\varepsilon,t)\rangle = \begin{pmatrix} |\Psi_I(t)\rangle \\ |\Psi_R(t)\rangle \\ |\Psi_A^{(\sigma|\delta)}(\varepsilon,t)\rangle \\ |\Psi_A^{\pi}(\varepsilon,t)\rangle \end{pmatrix}, \quad (6)$$

where we have split the contributions to the final ionic state $CO^+(A\,^2\Pi)$ produced by the emission of $\varepsilon(\sigma|\delta)$ electrons and those by the emission of $\varepsilon\pi$ electrons. We define the matrix

$$\hat{\mathbf{H}}(R,\theta,t) = \hat{\mathbf{T}}(R,\theta) + \begin{pmatrix} V_I(R) - \frac{i}{2}\Gamma_{\rm ph}(t) & \left[D_x^\dagger(t) - \frac{i}{2}W^\dagger(t)\right]\sin\theta & 0 & 0 \\ \left[D_x(t) - \frac{i}{2}W(t)\right]\sin\theta & V_R(R) - \frac{i}{2}[\Gamma_{\rm Aug} + \Gamma_*(t)] - \omega & 0 & 0 \\ d_x(t)\sin\theta & V & V_A(R) + \varepsilon - \omega & 0 \\ d_z(t)\cos\theta & 0 & 0 & V_A(R) + \varepsilon - \omega \end{pmatrix}. \quad (7)$$

With these notations, the final set of equations describing propagation of the nuclear wave packets Eq. (6) now takes on the following compact form:

$$i|\dot{\overline{\Psi}}(\varepsilon,t)\rangle = \hat{\mathbf{H}}(t)\,|\overline{\Psi}(\varepsilon,t)\rangle. \quad (8)$$

The matrix $\hat{\mathbf{H}}$ can be viewed as the effective Hamiltonian governing the two-dimensional nuclear dynamics in the considered RA decay process in an intense laser field. Below we summarize the physical meaning of each term of the Hamiltonian matrix (7) and provide their explicit expressions.

The $\hat{\mathbf{T}}(R,\theta)$ matrix is the common nuclear kinetic energy operator for the vibrational motion along the internuclear distance R and the rotational motion described by the angle θ between the polarization vector of the laser pulse and the molecular axis. The functions $V_I(R)$, $V_R(R)$, and $V_A(R)$ on the diagonal are the potential energies of the corresponding electronic states. The transitions between the electronic states are given by the following matrix elements of the total Hamiltonian Eq. (3)

$$\langle \Phi_R|\hat{H}(t)|\Phi_I\rangle = \langle 2\pi|\hat{x}|2\sigma\rangle \frac{\mathcal{E}_0\, g(t)}{2}\, e^{-i\omega t} = D_x(t)\, e^{-i\omega t}, \tag{9a}$$

$$\left\langle \Phi_A^{\varepsilon(\sigma|\delta)}\right|\hat{H}(t)|\Phi_R\rangle = \langle 2\sigma\ \varepsilon(\sigma|\delta)|1/\hat{r}_{12}|1\pi\ 2\pi\rangle = V, \tag{9b}$$

$$\left\langle \Phi_A^{\varepsilon(\sigma|\delta)}\right|\hat{H}(t)|\Phi_I\rangle = \langle \varepsilon(\sigma|\delta)|\hat{x}|1\pi\rangle \frac{\mathcal{E}_0\, g(t)}{2}\, e^{-i\omega t} = d_x(t)\, e^{-i\omega t}, \tag{9c}$$

$$\left\langle \Phi_A^{\varepsilon\pi}\right|\hat{H}(t)|\Phi_I\rangle = \langle \varepsilon\pi|\hat{z}|1\pi\rangle \frac{\mathcal{E}_0\, g(t)}{2}\, e^{-i\omega t} = d_z(t)\, e^{-i\omega t}. \tag{9d}$$

In Eqs. (9a), (9c), and (9d), the rotating wave approximation [25] has already been utilized, and, in contrast to the rapidly oscillating factor $e^{-i\omega t}$, the functions $D_x(t)$, $d_x(t)$, and $d_z(t)$ vary slowly on the timescale of $2\pi/\omega$. The matrix element Eq. (9a) describes the excitation of the resonant state via the x component of the dipole transition operator. The matrix element Eq. (9b) represents the Auger decay of the resonance into the final ionic state $CO^+(A\,^2\Pi)$ with the emission of $\varepsilon(\sigma|\delta)$ electrons, including both direct and exchange Coulomb integrals. The matrix elements (9c) and (9d) correspond to the direct ionization of the ground state into the final ionic state $CO^+(A\,^2\Pi)$ with the emission of $\varepsilon(\sigma|\delta)$ and $\varepsilon\pi$ electrons, respectively, via corresponding components of the dipole transition operator. Here and below, all transition matrix elements are assumed to vary slowly with the energy across the resonance and with the geometry within the Franck-Condon region and are replaced by their mean values.

The potential energy of the ground state (GS) $V_I(R)$ in the Hamiltonian matrix Eq. (7) is augmented by the imaginary time-dependent term $-\frac{i}{2}\Gamma_{\rm ph}(t)$, describing the leakage from the ground state due to its direct photoionization into all possible final ionic state (referred hereafter as "GS leakage" [4]). Its explicit expression was obtained in Ref. [4] in the local approximation [26,27] and reads

$$\Gamma_{\rm ph}(t) = 2\pi \sum_j \left|d^j_{x|z}(t)\right|^2, \tag{10}$$

where $d^j_{x|z}(t)$ are the dipole transition matrix elements for the direct ionization of the ground electronic state into all possible final ionic states numerated by superscript j and can be computed similarly to Eqs. (9c) and (9d). The total probability for the direct photoionization of the ground state (10) is identical to the quantity $\gamma_{\rm ph}(t)$ introduced in Ref. [2]:

$$\Gamma_{\rm ph}(t) = \gamma_{\rm ph}(t) = \sigma^{\rm tot}_{\rm ph} I(t)/\omega, \tag{11}$$

where $\sigma^{\rm tot}_{\rm ph}$ is the total direct photoionization cross section of the ground state at exciting-photon energy ω, $I(t)$ is the field intensity (2), and the quantity $I(t)/\omega$ stands in Eq. (11) for the photon flux.

Similarly, the total leakage from the resonance with "dressed" potential energy $V_R(R)-\omega$ is provided by the imaginary part $-\frac{i}{2}[\Gamma_{\rm Aug}+\Gamma_*(t)]$ on the respective diagonal element of $\hat{\mathbf{H}}$. The first term, $-\frac{i}{2}\Gamma_{\rm Aug}$, describes the usual time-independent leakage due to the Auger decay ("RA leakage" [4]). In the local approximation [26,27], the total rate for the Auger decay is given by Coulomb matrix element similar to Eq. (9b) as [24]

$$\Gamma_{\rm Aug} = 2\pi \sum_j |V_j|^2, \tag{12}$$

where the summation over index j runs over all possible RA decay channels. The second term, $-\frac{i}{2}\Gamma_*(t)$, is the time-dependent leakage due to the direct photoionization of the resonance ("RD leakage" [4]). As a good approximation [2,3], it can be chosen equal to GS leakage, $\Gamma_*(t)=\Gamma_{\rm ph}(t)$, since only outer electrons participate in the direct ionization of the ground state and the resonance at chosen x-ray photon energy ω.

As was demonstrated in Ref. [4], the usual direct coupling $D_x(t)$ between the ground state and the resonance through the laser field [1–3] is augmented by an additional time-dependent term $-\frac{i}{2}W(t)$, named leakage-induced complex coupling ("LIC coupling"). This term appears only if the photoionization from the ground state and Auger decay are simultaneously treated as required. Explicitly the LIC coupling reads [4]

$$W(t) = 2\pi \sum_j d^j_x(t) V^\dagger_j, \tag{13}$$

where the summation over index j runs over all possible final ionic states accessible by both channels. This is an indirect coupling that can be interpreted as follows: The photoelectron emitted by the ground state is recaptured by the residual ion to produce the resonance state, and reversely, the Auger electron can be captured by the residual ion, which then becomes the neutral atom in its ground state. The ground and "dressed" resonance states coupling (i.e., the matrix elements H_{12} and H_{21}) is non-Hermitian and operative as long as the pulse is on.

We note that the matrix elements of the permanent dipole moment of the CO molecule in the ground and resonance states must also be included in the respective diagonals of the Hamiltonian matrix Eq. (7). However, the permanent dipole moment of CO in its ground state is small. In addition, these matrix elements are proportional to the rapidly oscillating function $e^{-i\omega t}$, and the average effect of the permanent dipole moment on the pulse duration timescale is negligibly small. For simplicity, these matrix elements are not included in the present calculations.

The third row of the Hamiltonian matrix Eq. (7) describes the nuclear dynamics on the studied final ionic state produced via the emission of $\varepsilon(\sigma|\delta)$ electrons. The ionic state is populated by the direct photoionization from the ground state [matrix element $d_x(t)\sin\theta$] and coherently by the Auger decay of the resonance (matrix element V), all at a given kinetic energy ε of the emitted electron, and the created wave packet propagates on the "dressed" PESs $V_A(R)+\varepsilon-\omega$. The same

final ionic state can be produced by the direct ionization of the ground state via the emission of $\varepsilon\pi$ electron. This process is governed by the matrix element $d_z(t)\cos\theta$ in the forth row of the Hamiltonian matrix Eq. (7). The matrix element $H_{42} = 0$ indicates that the resonant population via the emission of $\varepsilon\pi$ electron is forbidden. Separating these two different kinds of processes into two different lines of the Hamiltonian matrix ensures that the corresponding wave packets accumulate on the PES of the $CO^+(A\,^2\Pi)$ ionic state incoherently (see also discussion above).

Finally, the nuclear wave packets $|\Psi_A^{(\sigma|\delta)}(\varepsilon,t)\rangle$ and $|\Psi_A^{\pi}(\varepsilon,t)\rangle$ contain the information on the RA electron spectrum for the production of the $CO^+(A\,^2\Pi)$ ionic state. The spectrum can be computed as the incoherent sum of the norms of the respective wave packets at long times [24]

$$\sigma_A(\varepsilon) = \lim_{t\to\infty}\left\langle \Psi_A^{(\sigma|\delta)}(\varepsilon,t)\middle|\Psi_A^{(\sigma|\delta)}(\varepsilon,t)\right\rangle + \lim_{t\to\infty}\left\langle \Psi_A^{\pi}(\varepsilon,t)\middle|\Psi_A^{\pi}(\varepsilon,t)\right\rangle. \quad (14)$$

B. Intersections of complex energy surfaces

As mentioned in the introduction, all parameters needed for the present calculations of the nuclear dynamics governed by the Hamiltonian matrix Eq. (7), such as the total and partial direct photoionization cross sections and the RA decay rates, as well as the oscillator strength for the resonant excitation, can be found in the literature. These parameters are collected in Table I. The potential energy curves of the ground, the resonant, and chosen final ionic states computed in Ref. [18] are depicted in the upper panel of Fig. 2. The vertical excitation energy from the initial state to the $v_r = 0$ vibrational level of the $C^*O(1s^{-1}\pi^*)$ resonance is $\omega = 287.4$ eV [15]. Of all levels, this level possesses the maximal excitation probability, which is about 87% [15,18]. The energy curve of the resonant state "dressed" by the field of this energy [i.e., $V_R(R) - \omega$] is also depicted in the upper panel of Fig. 2. One can see that this curve crosses the curve of the ground state in the Franck-Condon region (see also inset in this panel).

As has been demonstrated in Ref. [9], crossing of "dressed" by field states of a diatomic molecule results in the intersections of the corresponding two-dimensional complex PESs. It is well known [28,29] that for the formation of a conical intersection one needs at least two nuclear degrees of freedom whose changes affect the electronic wave function. These are not available for a free diatomic molecule. However, two dynamical variables R and θ enter the Hamiltonian matrix Eq. (7) explicitly and the rotation becomes the missing degree of freedom to allow for the formation of intersections for diatomics in the presence of a laser field. We point out that the rotational degree of freedom is involved in the nuclear dynamics only due to the presence of the laser field and only when the pulse is on. Very important, the nonadiabatic couplings, i.e., matrix elements of the nuclear momenta along R and θ, between the two "dressed" electronic states are singular at these intersections [30]. This gives rise to dramatic dynamical effects.

Without the on- and off-diagonal imaginary corrections to the Hamiltonian matrix Eq. (7), the two-dimensional potential energy surfaces of the "dressed" electronic states exhibit an intersection at $\theta = 0$ (coupling matrix elements H_{12} and H_{21} are proportional to $\sin\theta$). The impact of such light-induced conical intersections on the dynamics of a system has been recently demonstrated in Ref. [8]. Due to the presence of RA decay width, leakages, and LIC coupling in Eq. (7), the situation becomes more complicated. The two potential energy surfaces in R and θ space obtained by diagonalizing the electronic Hamiltonian $\hat{\mathbf{H}}(R,\theta,t) - \hat{\mathbf{T}}(R,\theta)$ in Eq. (7) are now complex and generally exhibit two intersecting points at which the real as well as the imaginary parts of the two electronic energies become degenerate [30]. This analog of a conical intersection in the continuum has been named doubly intersecting complex energy surfaces (DICES).

In order to illustrate the DICES appearing in the present case, we have diagonalized the complex electronic Hamiltonian. The "dressed" potential energy curves shown in the upper panel of Fig. 2 and parameters relevant for the RA decay of CO listed in Table I were utilized for the peak intensity of the laser pulse of $I_0 = 3\times10^{16}$ W/cm^2. The real and imaginary parts of the resulting surfaces are shown in Fig. 3. The projections of the real and imaginary seams of the complex intersecting surfaces onto the $R\theta$ plane are shown in the lower panel of Fig. 2. The seam of degeneracy of the real parts of the surfaces is shown by the solid line (see also inset for an enlarged scale). The imaginary parts of the surfaces have a complementary seam of degeneracy shown by the dashed line. The complex

TABLE I. Parameters for photoionization (PI) and resonant Auger (RA) decay of CO utilized in the present calculations. The energy of the exciting radiation is chosen to be $\omega = 287.4$ eV.

State	Quantity	Value
Ground state $1\sigma^2 2\sigma^2 3\sigma^2 4\sigma^2 1\pi^4 5\sigma^2\ X\,^1\Sigma^+$	Total direct PI cross section [11,12]	$\sigma_{\rm ph}^{\rm tot} = 0.24$ Mb
Resonance $1\sigma^2 2\sigma^1 3\sigma^2 4\sigma^2 1\pi^4 5\sigma^2 2\pi^1\,^1\Pi$	Total RA decay rate [22]	$\Gamma_{\rm Aug} = 80$ meV
	Oscillator strength [18]	$f = 0.158$ a.u.
Participator state $1\sigma^2 2\sigma^2 3\sigma^2 4\sigma^2 1\pi^3 5\sigma^2\ A\,^2\Pi$	Partial RA decay rates [18]	
	$\varepsilon\sigma$ channel	$\Gamma_{\rm Aug}^{A\varepsilon\sigma} = 1.07$ meV
	$\varepsilon\delta$ channel	$\Gamma_{\rm Aug}^{A\varepsilon\delta} = 3.46$ meV
	Partial direct PI cross sections [18]	
	$\varepsilon\sigma$ channel	$\sigma_{\rm ph}^{A\varepsilon\sigma} = 0.0060$ Mb
	$\varepsilon\pi$ channel	$\sigma_{\rm ph}^{A\varepsilon\pi} = 0.0105$ Mb
	$\varepsilon\delta$ channel	$\sigma_{\rm ph}^{A\varepsilon\delta} = 0.0185$ Mb

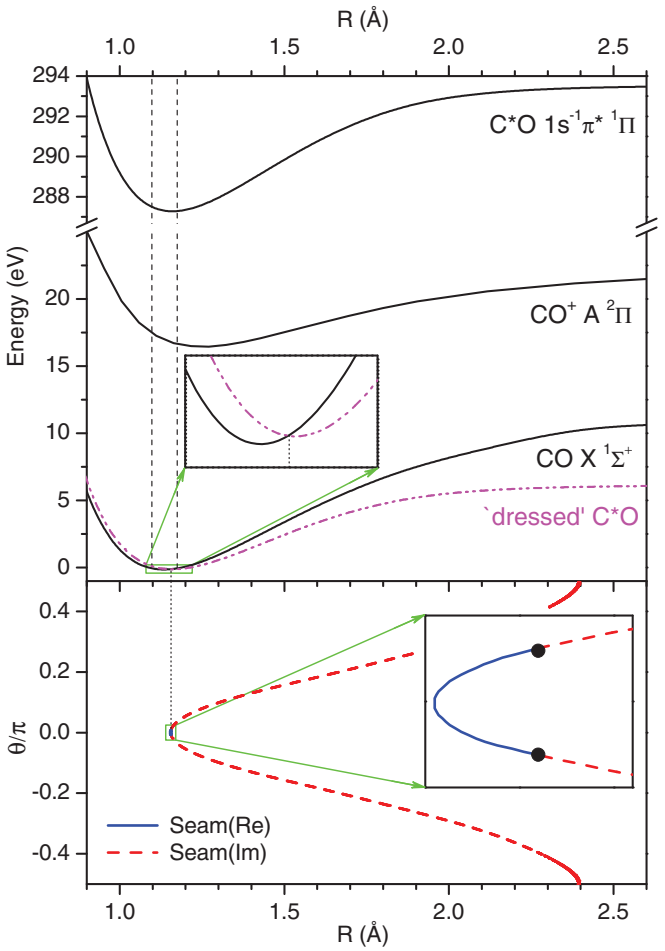

FIG. 2. (Color online) *Upper panel:* The potential energy curves of the ground $X\,^1\Sigma^+$ state of CO, the resonant state $C^*O(1s^{-1}\pi^*\,^1\Pi)$, and the final ionic state $CO^+(A\,^2\Pi)$ from Ref. [18], together with the curve of the resonant state "dressed" by the photon energy $\omega =$ 287.4 eV. The Franck-Condon region for the ground state of CO is marked by the vertical dashed lines, and the position of curve crossing is indicated by vertical doted line (see also inset). *Lower panel:* When the molecule is exposed to the x-ray laser field of peak intensity $I_0 = 3 \times 10^{16}$ W/cm^2, the ground and resonant potentials become doubly intersecting complex surfaces in R and θ space. Solid and dashed lines represent the projections of the real and imaginary seams of the complex intersecting surfaces onto the $R\theta$ plane. Two solid circles in the inset indicate the complex intersection points, where the real surfaces and the imaginary surfaces are simultaneously degenerate (see also Fig. 3).

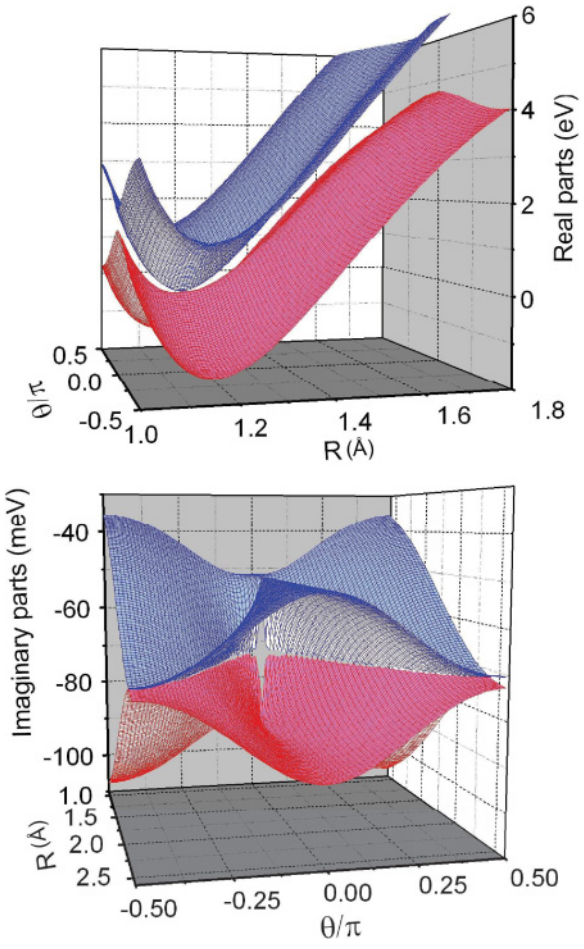

FIG. 3. (Color online) Real (upper panel) and imaginary (lower panel) parts of the resulting two-dimensional complex potential energy surfaces. The topology of the surfaces is that of doubly intersecting complex energy surfaces (DICES).

surfaces intersect at exactly two points, which are at the edges of the seams (solid circles in the inset). The present case fits well to the discussion of DICES considered in Ref. [30]. Finally, we note that the imaginary parts of the surfaces which reflect the decay of the resulting "dressed" states are now strongly dependent on R and θ [9,30] (see the lower panel of Fig. 3) in contrast to the initially constant values entering the Hamiltonian matrix Eq. (7).

III. RESULTS AND DISCUSSION

In order to illustrate the impact of DICES on the dynamics of the RA decay, we performed three sets of calculations to which we refer as models. The first model is the exact calculation, including both vibrational and rotational degrees of freedom in the nuclear dynamics [full Hamiltonian matrix (7)]. We refer to this model as the "DICES" model. In the second model, only the vibrational motion is allowed in the nuclear dynamics, eliminating thereby DICES (hereafter referred to as the "no DICES" model). To exclude rotations from the Hamiltonian matrix Eq. (7), we apply the common approach [8,31–33] incorporating rotational transitions via the selection rule $\Delta J = \pm 1$. The approximate Hamiltonian used for the vibrational dynamics of diatomics in laser fields can be obtained in this approach by replacing $\cos\theta$ and $\sin\theta$ functions in Eq. (7) by their optical transition matrix elements $\langle Y_{10}|\cos\theta|Y_{00}\rangle = \sqrt{\frac{1}{3}}$ and $\langle Y_{1\pm1}|\sin\theta|Y_{00}\rangle = \sqrt{\frac{2}{3}}$, respectively, where Y_{lm} are the usual spherical harmonics. In the third model (hereafter referred to as the "atomic" model), the whole nuclear dynamics is excluded from the calculations. For this purpose, the internuclear distance R is kept fixed at the position of the curves crossing (see Fig. 2) and $\cos\theta(\sin\theta)$ in Eq. (7) are replaced by their optical transition matrix elements as in the no DICES model.

Within all three models, we also study the individual contributions of different leakage mechanisms to the RA effect.

For this purpose, we performed the full calculations as well as calculations in which we take into account only one or two of the leakage mechanisms. We shall address the results of these systematic approximations to the three models as follows:

(i) Resonant—only the resonant channel is accounted for, i.e., all losses due to photoionization are neglected;

(ii) Direct—only the direct ionization channel is taken into account, i.e., the resonance state is excluded from the calculations;

(iii) Interference—both the direct and resonant channels and the interference between them are taken into account, but the resonance state itself cannot photoionize;

(iv) Total—all mechanisms are taken into account, including the direct photoionization of the resonance.

The present calculations were performed for Gaussian-shaped laser pulses of durations $\tau = 4,8$, and 16 fs, which are comparable to the RA decay lifetime of the C*O resonance of $\tau_d \approx 8.2$ fs. To be able to carry out the two-dimensional calculations on the coupled complex surfaces, we employed an efficient Multi Configuration Time Dependent Hartree (MCTDH) method [34] and code [35].

In order to evaluate the LIC coupling $W(t)$, one has to include the manifold of all final ionic states populated coherently via resonant and direct ionization channels [sum over index j in Eq. (13)]. These individual contributions of different final states to $W(t)$ can be different even by sign. In the absence of necessary data on all final ionic states, we have estimated and utilized in the calculations an upper bound of the true value of $W(t)$. For this purpose, we assumed that only one direct dipole transition amplitude $d_x(t)$ and only one Auger decay Coulomb matrix element V enter Eq. (13), which, however, correspond to the total direct photoionization cross section and to the total RA decay probability (Table I), respectively. Our computations shown below illustrate that for CO the impact of the LIC coupling is moderate for the field intensities investigated.

A. Total electron yield

The total electron yield as a function of the x-ray peak intensity calculated in the different models and approximations discussed above is depicted in Figs. 4, 5, and 6. In Fig. 4, the impact of DICES and nuclear dynamics in the presence of different leakage mechanisms is illustrated for a pulse duration of 8 fs. Figure 5 illustrates the impact of different leakage mechanisms within the DICES model for the same pulse duration. The total electron yield computed exactly [i.e., within the DICES model without approximations (Total)] is compared in Fig. 6 for different pulse durations. The total electron yield was computed as in [1,4] using

$$\lim_{t\to\infty}\sum_j \int d\varepsilon_j \langle \Psi_j(\varepsilon_j,t)|\Psi_j(\varepsilon_j,t)\rangle = 1 - \lim_{t\to\infty}\langle \Psi_I(t)|\Psi_I(t)\rangle, \tag{15}$$

where index j in the left-hand side of Eq. (15) must run over all possible final ionic states.

The atomiclike case, where the nuclear dynamics in R and θ space is excluded completely, is well understood [1,4]. In the resonant approximation within the atomic model, only

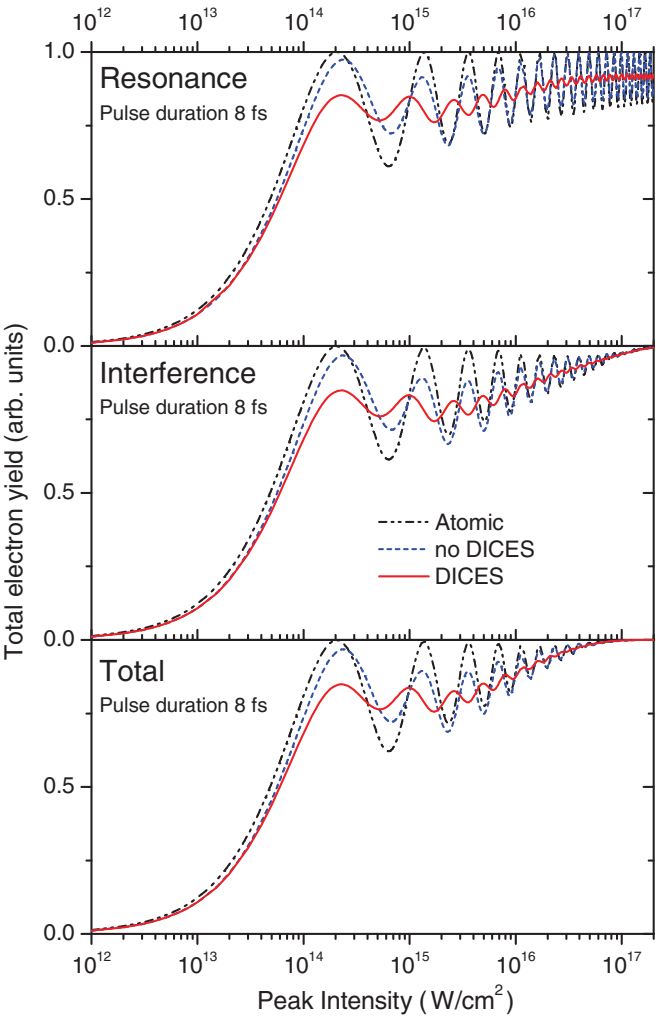

FIG. 4. (Color online) Total electron yield after exposure of CO to a coherent Gaussian-shaped pulse of duration 8 fs computed within different models and approximations discussed in the text. These include the atomiclike model (atomic; dash-dotted curves), rotation-free model (no DICES; dashed curves), and the exact model accounting for the vibrational and rotational degrees of freedom (DICES; solid curves). *Upper panel:* contribution of only the resonant channel (resonant). *Middle panel:* contribution of both the direct and resonant channels and the interference between them (interference). *Lower panel:* the contributions of all mechanisms including the direct photoionization of the resonance (total).

the Auger decay of the resonance and the Rabi oscillations between the resonance and the ground state are competing with each other. If the duration of the pulse is comparable or shorter than the Auger decay lifetime of the resonance and its intensity is low, the system has a finite probability of staying neutral after the laser pulse is over (dashed-dotted curve in the uppermost panel of Fig. 4; intensities below 10^{14} W/cm^2). At larger intensities, the field manages to transfer the whole population from the ground state into the resonance, and the atomiclike system can be completely ionized with the probability of 1. This situation corresponds to the half-completed Rabi cycles and to maxima in the total electron yield arriving at unity [1] (dashed-dotted curve in the uppermost panel of Fig. 4). At certain intensities, the atomic system manages to complete

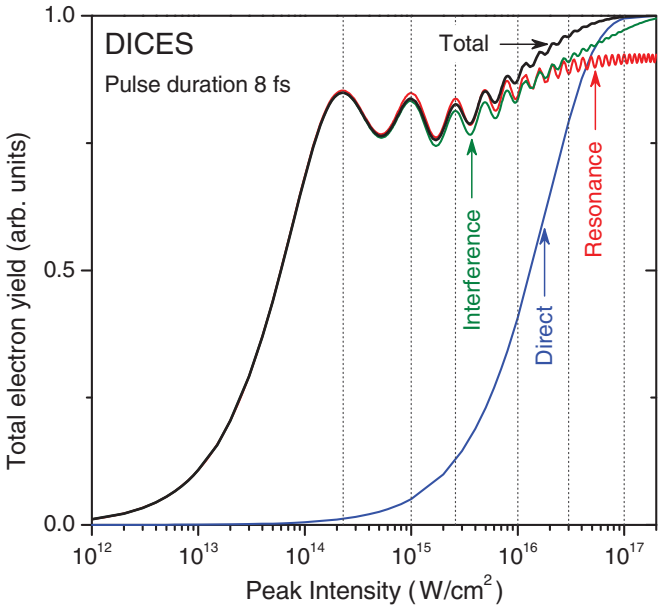

FIG. 5. (Color online) Total electron yield after exposure of CO to a coherent Gaussian-shaped pulse of duration 8 fs computed within the exact model, accounting for the vibrational and rotational degrees of freedom (DICES model). Shown are results of different approximations discussed in the text. These include the contribution of only the resonant channel (resonant), of only the direct ionization channel (direct), and of both the direct and resonant channels and the interference between them (interference), as well as the contributions of all mechanisms including the direct photoionization of the resonance (total). The vertical dotted lines indicate the peak intensities chosen for the calculation of the Auger spectra in Figs. 7 and 8.

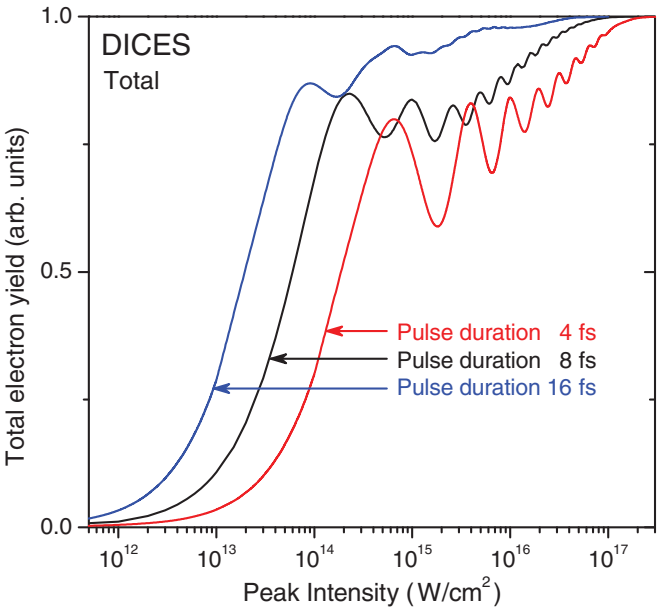

FIG. 6. (Color online) Total electron yield after exposure of CO to coherent Gaussian-shaped pulses of different durations (4, 8, and 16 fs) computed within the DICES model which accounts for the vibrational and rotational dynamics, employing the full formalism (total: no approximation).

several Rabi cycles during the pulse (to transfer the population back to the ground state) and the ionization probability drops again. These intensities correspond to the minima in the total yield.

In the resonance approximation for a molecule, the nuclear motion is additionally involved in the dynamics of the RA decay. As a result, the oscillations in the total electron yield possess much smaller amplitudes. Even in the no DICES model, where only R is the dynamical variable and θ is excluded from the dynamics, the difference from the atomic model is substantial [9] (cf. dash-dotted and dashed curves in the uppermost panel of Fig. 4). The maxima in the total electron yield are not necessarily touch unity (dashed curve). This is because a part of the energy of the absorbed photons is now transferred from the electronic degrees of freedom to the nuclear vibrational motion. The deviation from the atomic case is even more dramatic if we compare with the results of the full dynamics involving R and θ motions (DICES model). In the resonant approximation within this model, the complexity of the energy surfaces stems from the RA-leakage mechanism (Auger decay width) alone, and the appearing DICES are somewhat different [9] from the full case illustrated in the lower panel of Fig. 2. The seams of degeneracy of the real and imaginary parts of the surfaces belong to the straight line in the $R\theta$ plane but not to the contour (see also the original Ref. [30]). The strong nonadiabatic effects produced by the DICES couple the vibrational and the rotational degrees of freedom of a molecule, populating also rotational states of higher J (see discussion in subsection III C and Fig. 13 there, and also Refs. [7–9]). As a result, the Rabi oscillations are between superpositions of the rovibrational levels of two coupled electronic states. It is known that if more levels are involved in the dynamics, the Rabi oscillations are stronger damped. As one can see from Fig. 4, the oscillations in the total yield depicted by solid curves are now stronger damped than those computed in the rotation-free model (no DICES; dashed curves), where only Rabi oscillations between vibrational states of the molecule are considered. In the presence of DICES, the oscillations are strongly suppressed from below and from above, and the yield is always well below 1. In both atomic and no DICES models, the coupling matrix elements H_{12} and H_{21} in Eq. (7) carry the factor $\sqrt{\frac{2}{3}}$ after averaging over the rotational motion (i.e., by the optical transition matrix elements of $\sin\theta$). Therefore, periods of the oscillations in the total yield computed in these two models cover larger intervals of the field strength than in the DICES model.

The total electron yield computed in the direct approximation within the DICES model (blue curve in Fig. 5) illustrates the individual contribution of the GS leakage mechanism to the ionization process of the molecule. The total cross section for the ionization of the outer shells of CO ($\sigma_{\rm ph}^{\rm tot} = 0.24$ Mb; Table I) is much smaller than the probability for the ionization via the resonant channel. Thus, the total electron yield saturates to 1 due to the GS leakage at much larger intensities (at about 10^{17} W/cm^2) than in the resonant approximation. After its saturation, the direct ionization channel becomes comparable with the resonant one [4].

In the interference approximation within the DICES model (middle panel of Fig. 4, and also green line in Fig. 5), four

competitive mechanisms are present in the ionization of the molecule. These are the RA leakage and GS leakage discussed above, the interference between these two channels, and, of course, the wave packet nuclear dynamics on the strongly coupled PESs. The imaginary parts of the resulting complex intersecting energy surfaces are responsible for the leakages of the propagating wave packets. As is evident from the lower panel of Fig. 3, the resulting complex energy surfaces are strongly dependent on the dynamical variables and on all leakages. Consequently, a strict separation between the ionization mechanisms is impossible in the adiabatic picture. A simplified picture can, however, be suggested in the diabatic representation [before diagonalization of the electronic part of the Hamiltonian matrix (7)]. The nuclear wave packet propagates on the coupled complex surfaces of the ground and "dressed" resonant states. The parts of the wave packet, propagating on the resonant surface, decay into the final ionic state via the RA-leakage mechanism. The parts of the wave packet that propagate on the ground states surface decay via the GS leakage mechanism, i.e., direct photoionization. The competition between these two leakage mechanisms results in distinct modifications of the yield in all three models (middle panel of Fig. 4). The oscillations become less pronounced and saturate along the trend imposed by the direct approximation (cf. also green and red curves in Fig. 5). In the atomic model, not all of the oscillations arrive now at unity yield (dash-dotted curve in the middle panel of Fig. 4). This weak effect is a consequence of the complex coupling term (LIC coupling) [4]. The dramatic differences between the computed total yields shown in the middle panel of Fig. 4 illustrate the impact of the strongly coupled rovibrational motion via the DICES underlying the processes included in the interference approximation. The differences between the dash-dotted and dashed curves are due to the vibrational motion, and those between the dashed and solid curves are due to the rotational motion and DICES.

The photoionization of the resonance included in the RD-leakage mechanism enhances the ionization of the molecule (total calculations in the lowermost panel of Fig. 4; and also black curve in Fig. 5). It results in further losses of the wave packet propagating on the resonant surface, reducing its norm by the direct ionization of the resonance into preferably highly excited final ionic states. The oscillations in the total electron yield now become even less pronounced and saturate much earlier as a function of the laser intensity (cf. green and black curves in Fig. 5). We note that depending on the pulse duration and the parameters of the system, there is a certain interval of intensities where both the GS- and RD-leakage mechanisms are comparatively weak [4]. For the CO molecule exposed to a Gaussian pulse of 8 fs, these are the intensities up to about 10^{16} W/cm^2 (see Fig. 5). The total electron yields computed exactly [i.e., in the DICES model and without approximations (total)] for the three pulse durations of 4, 8, and 16 fs are compared in Fig. 6. For the shorter pulse of 4 fs, all leakages are weak up to about an intensity of 2×10^{16} W/cm^2, and for the longer pulse of 16 fs up to about an intensity of 5×10^{15} W/cm^2, which are twice larger and twice lower than the corresponding value of the 8 fs pulse, respectively. The dramatic effects of the DICES on the rovibrational dynamics persists also in the full calculations (cf. all curves in the lowermost panel of Fig. 4). The collective impact of all leakage mechanisms and of DICES results in a strong suppression of the oscillations of the total electron yield and in the saturation of the yield as a function of intensity, as illustrated in Fig. 5 by the black curve.

B. Resonant Auger spectrum

The RA electron spectra of the $CO^+(A\,^2\Pi)$ final ionic state at different peak intensities of the Gaussian-shaped pulse of 8 fs are depicted in Figs. 7 and 8, and those for the shorter (4 fs) and longer (16 fs) pulses in Figs. 9 and 10, respectively. Shown in these figures are the results of calculations performed within the two models (no DICES and DICES) without further

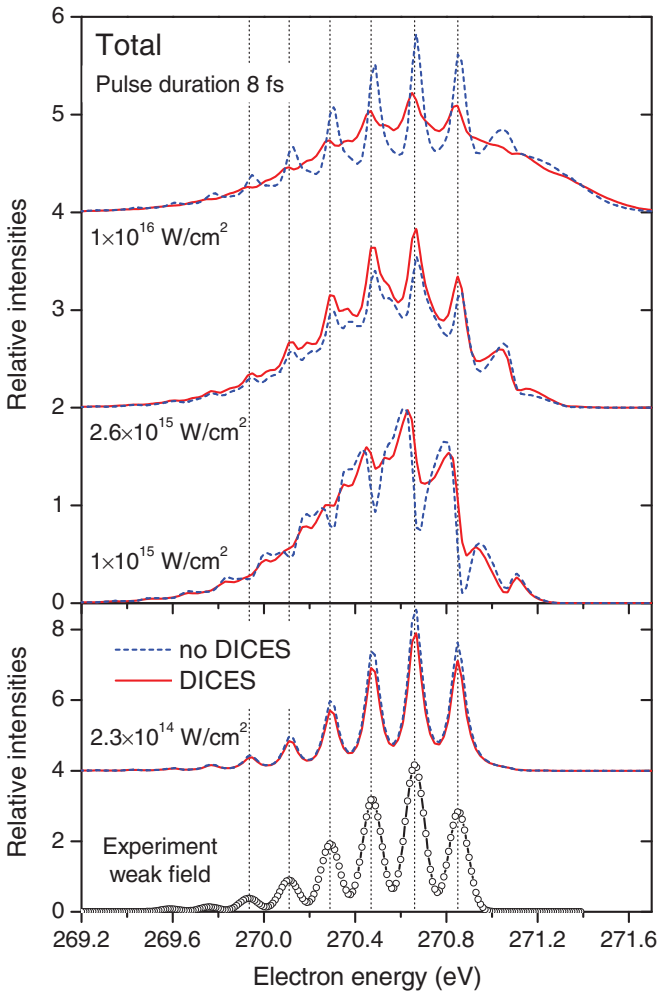

FIG. 7. (Color online) The RA electron spectra of CO for the Gaussian-shaped pulse of 8 fs duration computed employing the full formalism (total) within the two models: no DICES (broken curves) and DICES (solid curves). The peak intensities 2.3×10^{14} W/cm^2, 1×10^{15} W/cm^2, 2.6×10^{15} W/cm^2, and 1×10^{16} W/cm^2 chosen for the calculations are marked by the vertical dotted lines in Fig. 5. The weak-field experimental spectrum taken from Ref. [17] is shown for reference by open circles at the bottom. The electron energies corresponding to the energy positions of the v' vibrational levels of the $CO^+(A\,^2\Pi)$ state are marked by vertical dotted lines.

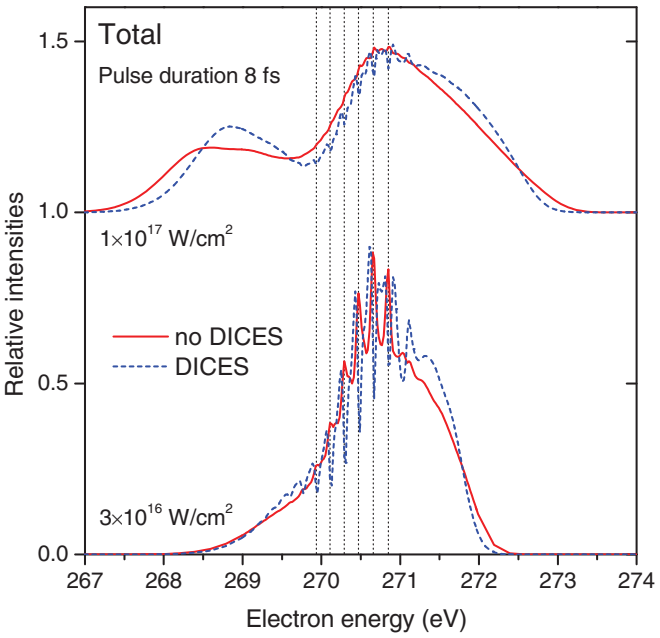

FIG. 8. (Color online) The RA electron spectra of CO for the Gaussian-shaped pulse of 8 fs duration computed employing the full formalism (total) within the two models: no DICES (broken curves) and DICES (solid curves). The peak intensities are 3×10^{16} W/cm^2 and 1×10^{17} W/cm^2 (see also notations in Fig. 7).

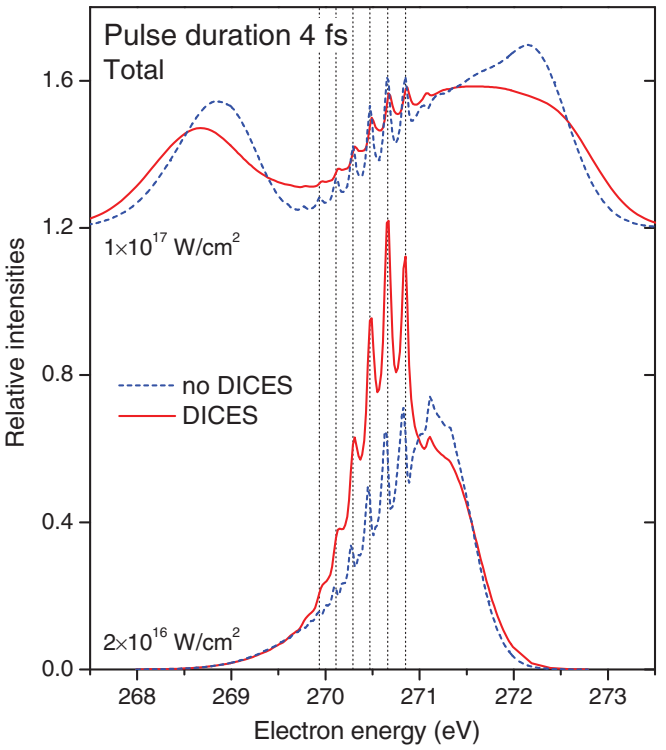

FIG. 9. (Color online) The RA electron spectra of CO for the Gaussian-shaped pulse of 4 fs duration computed employing the full formalism (total) within the two models: no DICES (broken curves) and DICES (solid curves). The peak intensities are 2×10^{16} W/cm^2 and 1×10^{17} W/cm^2.

approximations (total), i.e., with all leakage mechanisms and interference effects included. The experimental spectrum of Ref. [17] measured in the weak field utilized by synchrotron radiation is shown for reference at the bottom of Fig. 7 by open circles. One can see from the lower panel of Fig. 7 that in a weak field (see the two spectra computed within the no DICES and DICES models and peak intensity of 2.3×10^{14} W/cm^2): (i) the structure of the spectrum is independent of whether we have included DICES or not; (ii) the contribution of all leakage mechanisms due to direct photoionization is negligible; and (iii) the present theory well reproduces the experiment [17].

Let us first discuss the effect of DICES on the RA electron spectra in the presence of all leakages, as well as the trends in the RA spectrum induced by the field intensity and pulse duration. These are illustrated in Figs. 7–10. At field intensities beyond the first maximum in the total electron yield (Fig. 5), the stimulated emission from the resonance starts to compete with the RA decay, resulting in significant modifications of the electron line profiles. In atoms, the respective modifications consist in bifurcations of the RA electron peaks [1,4]. However, the situation in molecules is more complicated than in atoms due to the presence of many vibrational and rotational levels of each electronic state involved in the process. At an intensity of 1×10^{15} W/cm^2 (lowermost spectra in the upper panel of Fig. 7), the local minima in the line shapes appear at energies where maxima of the intensity were observed in the weak-field experiments, i.e., around the electron energies corresponding to the energy positions of the v' vibrational levels of the final ionic state marked by the vertical dotted lines in the figure. At a peak intensity of 2.6×10^{15} W/cm^2 (middle spectra in the upper panel of Fig. 7), the line shapes bifurcate again and their maxima again appear at their weak-field energies. However, relatively weak local maxima are now present in between the large maxima. Up to the peak intensity of 1×10^{16} W/cm^2 shown in Fig. 7, the effect of DICES is strongly visible, but there are no truly dramatic effects to be seen when comparing the no DICES and DICES models. The effect of DICES mainly consists in the broadening of the vibrational peaks and in the lowering of the intensities of the maxima in the spectrum (cf. solid and broken curves in Fig. 7 for all intensities).

At higher peak intensities (Figs. 8–10 for the 8 fs, 4 fs, and 16 fs pulses, respectively), a manifold of bifurcations of the line profiles has occurred. In addition, all leakage mechanisms evoked by the strong field contribute significantly to the computed spectra. As a result, the spectra are very different from the experimental one measured in weak fields [17]. The spectra cover much broader ranges of the electron energies. Very noteworthy is the appearance of the two-hump structure at the low- and high-energy sides at the largest field intensities considered here. It is produced by the strong direct ionization from the ground state, the influence of which grows rapidly with the field intensity [4] (see also the discussion around Fig. 11 at the end of this subsection). Obviously, the spectra exhibit many new features. Dramatic difference between the spectra computed within the no DICES and DICES models can be seen in Figs. 8–10. The spectra computed with and without accounting for the rotational motion (or with and without DICES) differ qualitatively in their structures, possessing different numbers of resonant features at different energy positions, dissimilar widths of peaks and even different relative

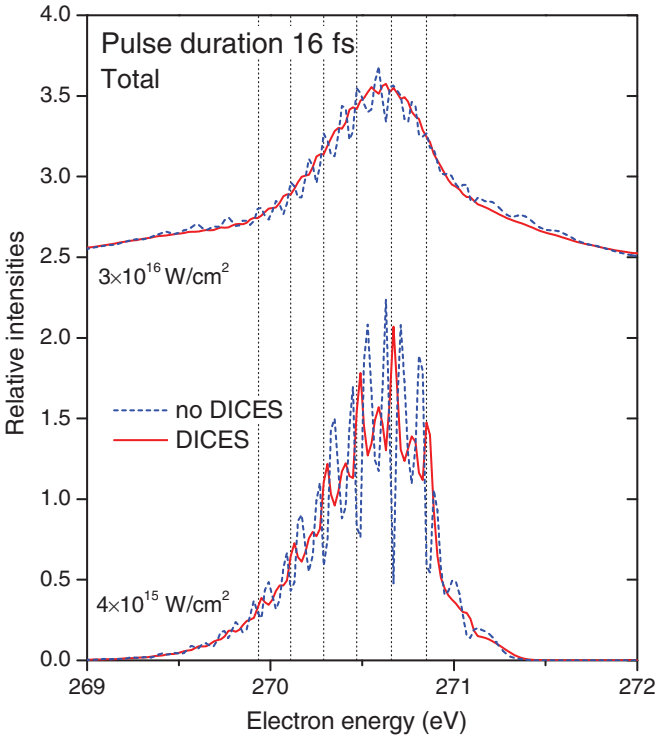

FIG. 10. (Color online) The RA electron spectra of CO for the Gaussian-shaped pulse of 16 fs duration computed employing the full formalism (total) within the two models: no DICES (broken curves) and DICES (solid curves). The peak intensities are 4×10^{15} W/cm^2 and 3×10^{16} W/cm^2.

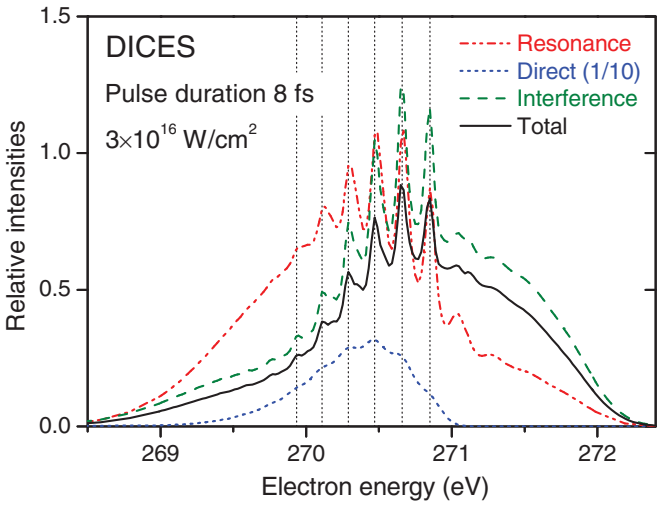

FIG. 11. (Color online) The RA electron spectra of CO for an 8 fs Gaussian-shaped pulse of 3×10^{16} W/cm^2 peak intensity computed within the DICES model (i.e., including rotations). Shown are the results of different approximations discussed in the text. These include the contribution of only the resonant channel (resonant; dash-dotted curve), of only the direct ionization channel (direct; dotted curve), and of both the direct and resonant channels and the interference between them (interference; dashed curve), as well as the contributions of all mechanisms including the direct photoionization of the resonance (total; solid curve). Note that the dotted curve is shown on a suppressed scale (factor 1/10) compared to the other curves.

intensity distributions among them. In some cases (see, e.g., the lower spectra in Figs. 8 and 10), the positions of local minima and maxima in the spectrum are even alternated.

Let us now discuss the individual contributions of the various leakage mechanisms to the exact RA electron spectra. Figure 11 depicts the spectra computed within the DICES model for the 8 fs pulse at the peak intensity of 3×10^{16} W/cm^2. The exact spectrum (total), of course, coincides with that shown in Fig. 8. The spectrum computed in the resonance approximation (i.e., in the presence of only RA decay) is depicted by the dash-dotted curve. As discussed above, at this field intensity, several bifurcations of each vibrational peak in the spectrum take place, and the resonant structure of the spectrum is wealthier than that observed in weak fields. The individual contribution of the direct photoionization from the ground state (GS leakage) is shown in the figure by the dotted curve. This contribution is enormous and the curve is shown on a strongly suppressed scale. Since there is no coupling between the ground and the final ionic states [see Eq. (7)], the line profile computed in the direct approximation remains unchanged with increasing laser intensity and, hence, displays no bifurcations. As demonstrated in Ref. [4], the intensity of the direct spectrum increases rapidly with the field intensity (see also Fig. 5). If the direct photoionization and resonant spectra were independent of each other, the direct ionization would be the dominant mechanism for the population of the $CO^+(A\,^2\Pi)$ final ionic state at this peak intensity (cf. dash-dotted and dotted curves in Fig. 11 and note the 1/10 factor).

Obviously, since the GS leakage intensifies with increasing field intensity, the role of the underlying interference effects in the spectrum also grows [4]. At the peak intensity of 3×10^{16} W/cm^2, the interference between the resonant and direct channels (interference approximation; dashed curve in Fig. 11) results in a surprisingly strong suppression of the direct ionization by the competing resonant pathway. The resulting distinct peak patterns in the RA spectrum possess strong asymmetry as seen by comparing the dash-dotted and dashed curves in the figure. With the present parameters utilized in the calculations (both the resonant and the direct electronic amplitudes have the same signs), the interference is more destructive on the low-electron-energy side than on the high-energy side. At larger intensities, the interference determines not only the shape of the computed RA spectra, but their integral intensities as well (see, e.g., the upper spectra in Figs. 8 and 9). However, as the total electron yield saturates as a consequence of the GS leakage mechanism, the impact of the interference effects saturates, too [4]. We note that strong interference effects persist also in the full (total) calculations (solid curve in Fig. 11), where the losses of the resonance due to photoionization is additionally taken into account. Depopulation of the resonance due to its ionization into other usually high-lying final ionic states results in an overall suppression of the spectrum without substantially changing its shape (cf. dashed and solid curves in the figure). At even higher intensity, however, the peaks seen in the middle of the spectrum will decrease and finally may practically become invisible as a consequence of the strong photoionization of the resonance state.

C. Impact of DICES on vibrations and rotations

Before the pulse arrived, the CO molecules have been in their ground rovibronic state CO($X\,^1\Sigma^+, v_0 = 0, J_0 = 0$), which implies that they were isotropically oriented. Figures 12 and 13 illustrate the change in the vibrational and rotational populations of the neutral molecules remaining in their ground electronic state after the 8 fs pulse has expired. In the no DICES model, where the rotational motion is excluded, the pulse couples only the electronic and vibrational degrees of freedom and the computed distribution of the neutral CO molecules over the rotational angle θ remains isotropic, represented by only the $J_0 = 0$ state. However, a part of the energy of absorbed photons is transferred from the electronic excitation to the vibrational ones. As one can see from Fig. 12 (no DICES model; broken curves), at the relatively low intensities below $I_0 = 10^{14}$ W/cm^2, the remaining neutral CO molecules stay mainly in the ground vibrational state $v_0 = 0$. As the field increases, the excitation of the $v_0 = 1$ vibrational state is possible. At the peak intensity of around 2.5×10^{14} W/cm^2, which correspond to the first maximum in the total electron yield computed in the same model (lower panel of Fig. 4), the populations of the $v_0 = 0$ and 1 vibrational levels become even comparable as can be seen by inspecting the broken curves in Fig. 12. At higher intensities, these populations oscillate: the maxima in the population of the $v_0 = 1$ state correspond to the maxima in the total electron yield depicted in the lower panel of Fig. 4 by the dashed curve. We notice that at the considered peak intensities, the population of the $v_0 = 2$ vibrational level is always below 1% and, therefore, is not shown in the figure.

Figure 13 illustrates the changes in the rotational distributions of the neutral molecules remaining in the $v_0 = 0$ and 1 vibrational levels of the ground electronic state after the pulse has expired. The impact of the light-induced nonadiabatic effects (DICES), which couples the vibrational and rotational degrees of freedom of the molecule, gives rise to the exchange of a very large number of angular momentum quanta during the ensuing dynamics. As a result, a wide range of rotational quantum numbers J_0 up to about $J_0 = 30$ is populated in the $v_0 = 0$ and 1 vibrational levels of the ground electronic state. The dipole transition selection rule of $\Delta J = \pm 1$ for each single absorbed or emitted photon ensures the population of only even J_0 rovibronic levels of the neutral molecules remaining in the ground electronic state after the pulse has expired. Figure 13 shows that higher and higher rotational states J_0 are excited with increasing field strength, and the populations of the rotational states possess oscillations with the peak intensity similar to the total electron yield (solid curve in the lower panel of Fig. 4). At the relatively low peak intensities below $I_0 = 10^{15}$ W/cm^2, only a few rotational states of small J_0 are excited. At higher peak intensities of around $I_0 = 10^{16}$ W/cm^2, the populations of low and high J_0 quantum numbers become

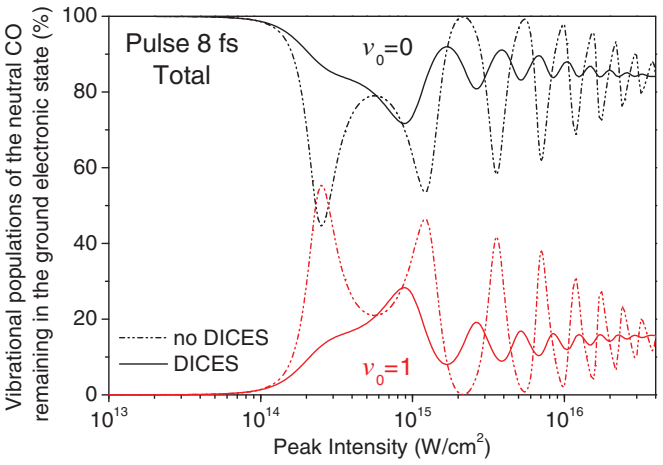

FIG. 12. (Color online) Impact of the DICES on the vibrational population of the neutral CO molecules remaining in its ground electronic state after the Gaussian-shaped pulse of 8 fs duration has expired. Shown are the populations of the $v_0 = 0$ and 1 vibrational levels as functions of the peak intensity, computed within the no DICES (broken curves) and DICES (solid curves) models (total: no approximations). At the considered peak intensities, the population of the $v_0 = 2$ vibrational level (not shown in the figure) is always well below 1%. The sum of the populations of all vibrational levels is normalized to 100% at each peak intensity.

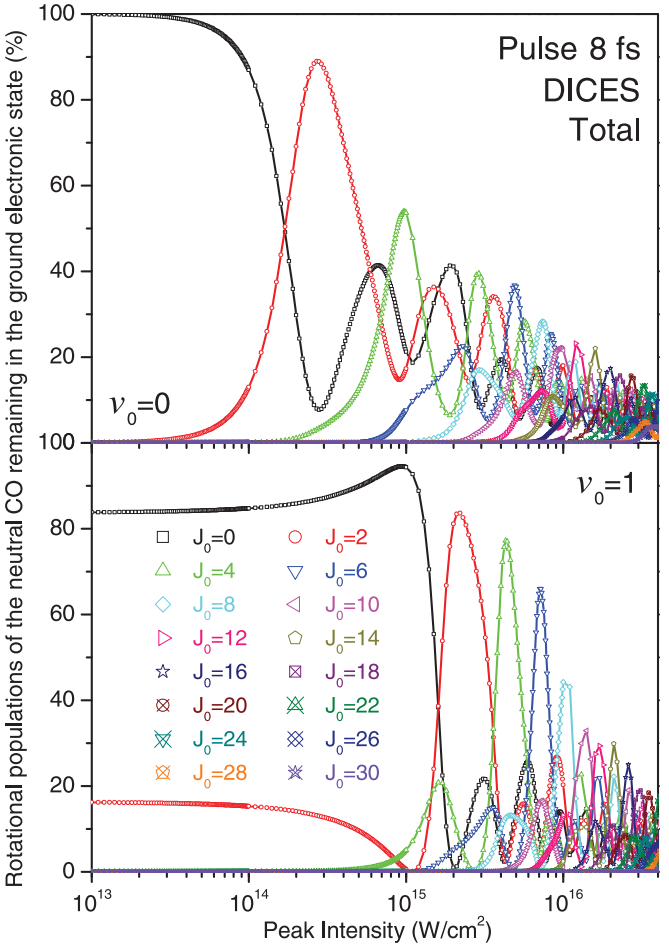

FIG. 13. (Color online) Impact of the DICES on the rotational population of the neutral CO molecules remaining in its ground electronic state after the Gaussian-shaped pulse of 8 fs duration has expired. Shown are the populations of the J_0 rotational levels for the $v_0 = 0$ (upper panel) and $v_0 = 1$ (lower panel) vibrational levels as a function of the peak intensity computed exactly (i.e., DICES model and total). For each vibrational level v_0, the sum of the populations of all rotational levels is normalized to 100% at each peak intensity.

comparable. The excitation of higher rotational states J_0 results in a strongly anisotropic distribution of the neutral molecules over the rotational angle θ after the pulse is over. We remind that in the no DICES model, the distribution over the rotational angle θ for the ground electronic state remains isotropic as only $J_0 = 0$ appears. The coupling between the vibrational and rotational degrees of freedom via DICES changes also the vibrational populations of the residual neutral molecules, as demonstrated by the solid curves in Fig. 12. The oscillations in the vibrational populations become less pronounced (cf. solid and broken curves for each vibrational state v_0 in the figure). The maxima in the population of the $v_0 = 1$ state correspond now to the maxima in the total electron yield computed in the same model (solid curve in the lower panel of Fig. 4).

The impact of the DICES on the nuclear dynamics is also documented in the distributions of ions [9], e.g., in the final $CO^+(A\,^2\Pi)$ electronic state of interest (not shown in the paper). This effect is, however, difficult to measure owing to the following reasons. First of all, these rotational distributions of the final ionic states are different for each energy of the emitted RA electron, and coincidence techniques must be applied. In addition, the ions resulting from the RA decay can be further ionized by the strong pulse, and, as a consequence, taken away from the coincidence signal.

IV. CONCLUSIONS

The resonant Auger decay of the core-excited $C^*O(1s^{-1}\pi^*, v_r = 0)$ molecule into the final ionic state $CO^+(A\,^2\Pi)$ in an intense x-ray laser field is studied theoretically. The mechanisms responsible for the dynamics of the process are incorporated in the calculations. In particular, we investigated the impact of the light-induced nonadiabatic coupling between the vibrational and rotational degrees of freedom of a diatomic molecule caused by the analog of the conical intersections of the complex energy surfaces of the ground and "dressed" resonant electronic states (briefly, by the light-induced DICES). The nonadiabatic nuclear wave packet dynamics accompanying the process competes with different ionization mechanisms of the molecule evoked by the laser field: direct ionizations of the ground state (GS leakage), the resonance (RD leakage), and the Auger decay of the resonance (RA leakage).

The dynamics of the RA process of a diatomic molecule exposed to strong x-ray pulses is completely different from that predicted for atomic systems, due to the presence of the nuclear degrees of freedom. In the adiabatic representation, the two-dimensional nuclear wave packet propagates on the complex (owing to the various leakages) potential energy surfaces of the ground and "dressed" resonant states. Being coupled by the non-Hermitian interaction induced by the laser field and by the RA decay, these complex surfaces become doubly intersecting in R and θ space (DICES; doubly intersecting complex energy surfaces). The nonadiabatic couplings at these intersection points are singular, resulting in strong coupling between the electronic, vibrational, and rotational degrees of freedom. The imaginary parts of the resulting intersecting complex surfaces, responsible for leakages of the nuclear wave packets from the surfaces, are strongly dependent on both R and θ. As a result, one cannot anymore make a clear separation between the involved leakage mechanisms. Finally, we remind that the finite pulse duration enforces an explicitly time-dependent picture of the process.

The individual impacts of the different underlying mechanisms on the dynamics of the process are illustrated on observable quantities like the total electron yield, the RA electron spectra, and the vibrational and rotational distributions of the neutral molecules remaining in the ground electronic state after the pulse is over. Interference effects and the effects of the competition between the different leakage mechanisms are identified and discussed. These leakage and interference effects increase with the field strength. The nonadiabatic effects result in dramatic changes of the computed total electron yield and electron spectra. These changes are not only of quantitative but also of unexpectedly strong qualitative nature and can be verified experimentally. Finally, although the initial rotational distribution has been chosen to be isotropic, the energy exchange between the vibrational and the rotational degrees of freedom via the light-induced DICES results in strongly nonhomogeneous angular distributions of the neutral molecules surviving the pulse and of the ions produced. In the absence of the nonadiabatic effects these distributions would remain isotropic as initially prepared.

The controllability of the light-induced DICES, i.e., of the location of the intersection by laser frequency and of the strength of the interstate coupling by the field intensity, makes the investigation in intense fields of the resonance Auger process and of decay processes in general a challenging and promising new area of research.

ACKNOWLEDGMENTS

The authors thank H.-D. Meyer for his assistance in running the MCTDH package and A.I. Kuleff for many fruitful discussions. Y.–C.C. acknowledges the International Max Planck Research School for Quantum Dynamics in Physics, Chemistry and Biology (IMPRS-QD) for financial support. Financial support by the DFG is gratefully acknowledged.

[1] N. Rohringer and R. Santra, Phys. Rev. A **77**, 053404 (2008).
[2] J.-C. Liu, Y.-P. Sun, C.-K. Wang, H. Ågren, and F. K. Gel'mukhanov, Phys. Rev. A **81**, 043412 (2010).
[3] Y.-P. Sun, J.-C. Liu, C.-K. Wang, and F. K. Gel'mukhanov, Phys. Rev. A **81**, 013812 (2010).
[4] Ph. V. Demekhin and L. S. Cederbaum, Phys. Rev. A **83**, 023422 (2011).
[5] P. Emma *et al.*, Nature Photonics **4**, 641 (2010).
[6] L. Young *et al.*, Nature (London) **466**, 56 (2010).
[7] N. Moiseyev, M. Šindelka, and L. S. Cederbaum, J. Phys. B **41**, 221001 (2008).

[8] M. Šindelka, N. Moiseyev, and L. S. Cederbaum, J. Phys. B **44**, 045603 (2011).
[9] L. S. Cederbaum, Y.-C. Chiang, Ph. V. Demekhin, and N. Moiseyev, Phys. Rev. Lett. **106**, 123001 (2011).
[10] C. M. Truesdale, D. W. Lindle, P. H. Kobrin, U. E. Becker, H. G. Kerkhoff, P. A. Heimann, T. A. Ferrett, and D. A. Shirley, J. Chem. Phys. **80**, 2319 (1984).
[11] O. Hemmers, in *Studies of Vacuum Ultraviolet and X-Ray Processes*, edited by U. Becker (AMS Press, New York, 1993), Vol. 3.
[12] U. Becker and D. Shirley, *VUV and Soft X-Ray Photoionization* (Plenum Press, New York, 1996), Chap. "Partial Cross Section and Angular Distribution," pp. 135–180.
[13] G. Prümper, D. Rolles, H. Fukuzawa, X. J. Liu, Z. Pešic, I. Dumitriu, R. R. Lucchese, K. Ueda, and N. Berrah, J. Phys. B **41**, 215101 (2008).
[14] V. Carravetta, F. K. Gel'mukhanov, H. Ågren, S. Sundin, S. J. Osborne, A. Naves de Brito, O. Björneholm, A. Ausmees, and S. Svensson, Phys. Rev. A **56**, 4665 (1997).
[15] M. N. Piancastelli, M. Neeb, A. Kivimäaki, B. Kempgensy, H. M. Köppe, K. Maier, A. M. Bradshaw, and R. F. Fink, J. Phys. B **30**, 5677 (1997).
[16] S. J. Osborne, S. Sundin, A. Ausmees, S. L. Sorensen, A. Kikas, and S. Svensson, J. Electron Spectrosc. Relat. Phenom. **95**, 25 (1998).
[17] E. Kukk, J. D. Bozek, W. Cheng, R. F. Fink, A. A. Wills, and N. Berrah, J. Chem. Phys. **111**, 9642 (1999).
[18] Ph. V. Demekhin, I. D. Petrov, V. L. Sukhorukov, W. Kielich, P. Reiss, R. Hentges, I. Haar, H. Schmoranzer, and A. Ehresmann, Phys. Rev. A **80**, 063425 (2009); **81**, 069902(E) (2010).
[19] Z. W. Gortel, R. Teshima, and D. Menzel, Phys. Rev. A **58**, 1225 (1998).
[20] S. Bonhoff, K. Bonhoff, and K. Blum, J. Phys. B **32**, 1139 (1999).
[21] R. F. Fink, M. N. Piancastelli, A. N. Grum-Grzhimailo, and K. Ueda, J. Chem. Phys. **130**, 014306 (2009).
[22] K. C. Prince, M. Vondráček, J. Karvonen, M. Coreno, R. Camilloni, L. Avaldi, and M. de Simone, J. Electron Spectrosc. Relat. Phenom. **101–103**, 141 (1999).
[23] F. K. Gel'mukhanov, L. N. Mazalov, and A. V. Kondratenko, Chem. Phys. Lett. **46**, 133 (1977).
[24] E. Pahl, H.-D. Meyer, and L. S. Cederbaum, Z. Phys. D **38**, 215 (1999).
[25] D. J. Griffiths, *Introduction to Quantum Mechanics* (Prentice-Hall, New Jersey, 1994).
[26] L. S. Cederbaum and W. Domcke, J. Phys. B **14**, 4665 (1981).
[27] W. Domcke, Phys. Rep. **208**, 97 (1991).
[28] W. Domcke, D. R. Yarkony, and H. Köppel (eds.), *Conical Intersections* (World Scientific, Singapore, 2004).
[29] M. Baer, *Beyond Born-Oppenheimer: Electronic Non-adiabatic Coupling Terms and Conical Intersections* (Wiley Interscience, Wiley and Sons, Hoboken NJ, 2006).
[30] S. Feuerbacher, T. Sommerfeld, and L. S. Cederbaum, J. Chem. Phys. **120**, 3201 (2004).
[31] R. Lefebvre, O. Atabek, M. Šindelka, and N. Moiseyev, Phys. Rev. Lett. **103**, 123003 (2009).
[32] V. S. Prabhudesai *et al*., Phys. Rev. A **81**, 023401 (2010).
[33] O. Atabek, R. Lefebvre, and F. X. Gadéa, Phys. Rev. A **74**, 063412 (2006).
[34] H.-D. Meyer, U. Manthe, and L. S. Cederbaum, Chem. Phys. Lett. **165**, 73 (1990).
[35] G. A. Worth, M. H. Beck, A. Jäckle, and H. Meyer, *The Multi-Configuration Time–Dependent Hartree (MCTDH) Package*, see [http://www.pci.uni-heidelberg.de/cms/mctdh.html].